Breast Cancer Research

RESEARCH

Open Access

Atypical cell cycle regulation promotes mammary stem cell expansion during mammary development and tumourigenesis

Bre-Anne Fifield[1,2], John Vusich[3], Erika Haberfellner[4], Eran R. Andrechek[3] and Lisa A. Porter[1,2,5*]

Abstract

Background The cell cycle of mammary stem cells must be tightly regulated to ensure normal homeostasis of the mammary gland to prevent abnormal proliferation and susceptibility to tumorigenesis. The atypical cell cycle regulator, Spy1 can override cell cycle checkpoints, including those activated by the tumour suppressor p53 which mediates mammary stem cell homeostasis. Spy1 has also been shown to promote expansion of select stem cell populations in other developmental systems. Spy1 protein is elevated during proliferative stages of mammary gland development, is found at higher levels in human breast cancers, and promotes susceptibility to mammary tumourigenesis when combined with loss of p53. We hypothesized that Spy1 cooperates with loss of p53 to increase susceptibility to tumour initiation due to changes in susceptible mammary stem cell populations during development and drives the formation of more aggressive stem like tumours.

Methods Using a transgenic mouse model driving expression of Spy1 within the mammary gland, mammary development and stemness were assessed. These mice were intercrossed with p53 null mice to study the tumourigenic properties of Spy1 driven p53 null tumours, as well as global changes in signaling via RNA sequencing analysis.

Results We show that elevated levels of Spy1 leads to expansion of mammary stem cells, even in the presence of p53, and an increase in mammary tumour formation. Spy1-driven tumours have an increased cancer stem cell population, decreased checkpoint signaling, and demonstrate an increase in therapy resistance. Loss of Spy1 decreases tumor onset and reduces the cancer stem cell population.

Conclusions This data demonstrates the potential of Spy1 to expand mammary stem cell populations and contribute to the initiation and progression of aggressive, breast cancers with increased cancer stem cell populations.

Keywords Mammary stem cells, Cell cycle, Mammary gland development, Breast cancer, Breast cancer stem cells

*Correspondence:
Lisa A. Porter
lporter@uwindsor.ca
[1]Department of Biomedical Sciences, University of Windsor, Windsor, ON N9B 3P4, Canada
[2]WE-SPARK Health Institute, University of Windsor, Windsor, ON N9B 3P4, Canada
[3]Department of Physiology, Michigan State University, East Lansing, MI, United States of America
[4]Schulich School of Medicine and Dentistry, Western University, London, ON, Canada
[5]St. Joseph's Health Care London, Lawson Health Institute, London, ON N6A 4V2, Canada

Introduction

The mammalian mammary gland is a hormone-sensitive organ that undergoes complex structural and functional changes throughout life to permit lactogenesis. During puberty, pregnancy and through estrous, cell cycle activators support cell proliferation and expansion of the mammary epithelium [1–5]. Mammary cells are guided by morphological cues to form a branching ductal network with proliferation balanced by apoptosis as well as differentiation down luminal or myoepithelial lineages [6, 7]. A perfect balance of these events is required to ensure proper structure and organization of the mature, functional adult mammary gland. Aberrant regulation of mediators controlling these events may initiate or support tumourigenesis.

Mammary **s**tem **c**ells (MaSCs) and progenitor populations within the gland have been proposed as the cells of origin for many breast cancers [8–10]. Tight regulation over the expansion and differentiation of MaSCs throughout mammary development depends on the production and destruction of cell cycle mediators as well as tumour suppressors such as p53. Loss of p53 promotes a switch from asymmetric to symmetric division of stem and progenitor cells, and results in susceptibility to tumourigenesis [11–14]. Resolving the molecular mediators of mammary stem and progenitor populations throughout development is key to understanding how breast cancer initiates and progresses.

The atypical cell cycle mediator, Spy1 (also referred to as SpeedyA1, RINGO; gene *SPDYA*), is tightly regulated throughout mammary development, with protein levels being high during proliferative and regenerative phases and downregulated during differentiation [15]. Spy1 promotes cell cycle progression through both G1/S and G2/M by uniquely binding and activating both **C**yclin **D**ependent **K**inase (Cdk)1 and Cdk2 [16–18]. Unlike classical cyclin proteins, Spy1 activates Cdks independent of canonical post-translational modifications including phosphorylation of the Cdk T-loop by the Cyclin Activated Kinase (Cak) [19]. Previous work has elucidated a novel negative feedback loop in healthy cells between Spy1 and p53, where p53 promotes Spy1 degradation and supports a cell cycle arrest [20]. Sustained Spy1 expression occurs in the absence of p53 and overrides cell cycle checkpoints and promotes oncogenic transformation of human cell lines [21–25]. Driving Spy1 with a MMTV promoter on a mammary tumour resistant background (B6CBAF1/J) increases susceptibility to carcinogen-induced mammary tumorigenesis [20]. This occurs, at least in part, by overriding p53-mediated checkpoints allowing for accumulation of DNA damage, hence supporting that a Spy1-p53 feedback loop plays a critical role in mediating breast cancer susceptibility [20]. Spy1 protein levels are elevated in cases of human breast cancer as well as in other cancers including brain, liver, ovarian, and several blood cancers [21, 26–30] and elevated levels of Spy1 drives more aggressive, drug resistant disease in both **E**strogen **R**eceptor (ER) positive and Triple Negative Breast Cancer [26, 31]. Several publications have implicated Spy1 in expanding normal and cancer stem cell populations in the brain [28, 32, 33]. Recently, Spy1 has been shown to activate the epigenetic regulator EZH2 and support reprogramming to a pluripotent state [34]. Whether Spy1-mediated effects on stemness have any implications in the mammary gland was not previously addressed.

Herein we provide the first data demonstrating that overexpression of Spy1 within the mouse mammary gland alters mammary ductal development and promotes functional characteristics of MaSCs. We have previously shown that Spy1 cooperates with loss of p53 to increase susceptibility to tumourigenesis and confirm this finding on a mouse background sensitive to mammary tumourigenesis. Dissecting this further, we provide evidence that Spy1 driven tumours have increased stem cell and cell cycle progression signaling potentially contributing to increased therapy resistance, linking early changes in mammary development to tumourigenic properties. This work adds to the growing literature supporting a role for this atypical cell cycle mediator in mammary gland development and breast tumourigenesis. More broadly this work provides a novel mechanistic connection between expansion of MaSC populations and breast cancer initiation, progression, and response to therapy.

Materials and methods

Generation and maintenance of MMTV-Spy1 transgenic mice

MMTV-Spy1 transgenic mice were generated as described [20] and backcrossed 10 generations onto an FVBN/J background. Routine genotyping was performed as described [20]. The p53 knockout mouse, B6.129S2-Trp53tm1Tyj/J, was purchased from Jackson Laboratory (002101) [35] and backcrossed 10 generations onto an FVBN/J background. Estrous cycle was assessed in all mice at the time of sample collection using established protocols [36]. Mice were maintained following the Canadian Council of Animal Care guidelines under animal utilization protocol 20−15 approved by the University of Windsor. The maximum allowed tumour volume of $1.5cm^3$ was not exceeded in any of the described studies according to protocol guidelines.

Mammary fat pad transplantation and limiting dilution assay

For limiting dilution assays of normal mammary epithelial cells, mammary epithelial cells were isolated from 8-week-old and 6-month-old MMTV-Spy1 or

FVBN/J littermate control mice as described [37]. Cells were transplanted into the cleared glands of 3-week-old FVBN/J mice and successful clearing was monitored via the addition of a cleared gland with no injected cells. For limiting dilution assays of primary tumour cells, cells were transplanted into the inguinal mammary glands of 6-week-old FVBN/J mice. Mammary epithelial cells from intercrossed MMTV-Spy1 and p53 null 8-week-old mice were transplanted into the cleared glands of 3-week-old FVBN/J mice for tumour studies and successful clearing was monitored via addition of cleared gland with no injection. Analysis was performed as described [38].

Whole mount analysis

Inguinal mammary glands were placed on positively charged slides and incubated in Clarke's Fluid (75% ethyl alcohol 25% acetic acid) overnight. The following day, slides were placed in 70% ethyl alcohol for 30 min and stained for a minimum of overnight in carmine alum (0.2% carmine, 0.5% potassium aluminium sulphate). Glands were placed in destain solution (1%HCl, 70% ethyl alcohol) for 4 to 6 h and dehydrated in a series of ascending alcohol concentrations (70%, 95%, 100%) for 15 min each prior to clearing of the gland overnight in xylene. Slides were mounted with Permount Toluene (Fisher Scientific) solution prior to imaging.

Histology and immunostaining

Tissue was collected and fixed in 10% neutral buffered formalin and immunohistochemistry was performed as described [39]. Primary antibodies were as follows: Spy1 (1:200; PA5-29417; Thermo Fisher Scientific), PCNA (1:500; sc-9857; Santa Cruz); cleaved caspase-3 (1:250; 9661; Cell Signaling), cytokeratin 8 (1:100; MABT329 Millipore), phospho-histone H3 S10 (1:300; ab5176 Abcam) and smooth muscle actin (1:250; A2547 Sigma). Slides were imaged using the LEICA DMI6000 inverted microscope with LAS 3.6 software.

Quantitative real time PCR analysis

RNA was isolated using the Qiagen RNeasy Plus Kit following manufacturer's instructions. Equal amounts of cDNA were synthesized using Quanta qScript Master Mix as per manufacturer's instructions. Real time PCR was performed using SYBR Green detection (Applied Biosystems) and was performed and analysed using Viia7 Real Time PCR System (Life Technologies) and software.

Immunoblotting

Tissue was lysed as previously described [20]. Protein concentrations were determined via Bradford assay as per manufacturer instructions and equal amounts of protein were separated using SDS-PAGE and transferred to PVDF membrane. Membranes were blocked in 1% BSA for 1 h at room temperature and incubated in primary antibody overnight at 4 °C (Actin 1:1000 (MAB1501; Millipore), p53 1:1000 (ab131442; Abcam)). Secondary antibody was used at a concentration of 1:10,000 for 1 h at room temperature and chemiluminescent peroxidase substrate (BioRad) was used for visualization as per manufacturer instructions. Images were captured using Bio-Rad ChemiDoc Imaging System.

Primary mammary epithelial cell culture

Mammary epithelial cells (MECs) were isolated from inguinal mammary glands as previously described [37] and cultured at 5% CO_2 at 37 °C in DMEM/F12 supplemented with 10% FBS, 5 µg/mL insulin, 1 µg/mL hydrocortisone, 10ng/mL EGF and 1% P/S for adherent culture, and were sub-cultured using 0.05% trypsin. For mammosphere formation assays, cells were seeded at a density of 10,000–20,000 cells per mL of culture media (DMEM/F12 supplemented with 20ng/mL bFGF, 20ng/mL EGF, B27, 100 µg/mL gentamicin, 1%P/S) in ultra low attachment plates. Mammospheres were dissociated with 0.05% trypsin to obtain single cell suspensions and seeded at a density of 1,000–5,000 cells/mL for secondary sphere formation. Transfection of primary MECs with sip53 (Santa Cruz) and siRNA control (Santa Cruz) was performed using siRNA Transfection Reagent as per manufacturer's instructions. For treatment assays, cells were seeded at a density of 20,000 cells per well in a 24 well plate and treated with vehicle control (DMSO), 25nM doxorubicin, 6mM cyclophosphamide, 100nM paclitaxel, 10nM dinaciclib or 500nM palbociclib.

PKH staining

Primary MECs were stained with PKH26 dye (Sigma) as per manufacturer's instructions and seeded for mammosphere formation assays to obtain primary mammospheres. Primary mammospheres were dissociated into single cell suspensions and sorted based on PKH26 staining intensity using a BD FACSARIA Fusion flow cytometer where single cell suspensions were then seeded for secondary sphere formation.

Flow cytometry

Primary MECs were isolated as described [37] and epithelial cells were enriched using the EasySep Mouse Epithelial Cell Enrichment Kit (Stem Cell Technologies) as per manufacturer's instructions. Cells were stained with EpCAM-APC (BD Bioscience 563,478) and CD49f-Superbright 436 (Thermo 62-0495-82) and FACS was performed using a BD LSR Fortessa X-20 (Becton Dickinson).

RNA-sequencing and gene expression analysis

Total RNA was isolated using the Qiagen RNeasy Plus Kit following manufacturer's instructions. RNA was sent to Psomagen and quality measured using Agilent 2100 Expert Eukaryote Total RNA NanoDrop. RNA libraries were prepared using TruSeq Stranded mRNA Library Prep Kit. Libraries were sequenced using the S4 chipset on the NovaSeq6000 instrument (Illumina) for 150 bp paired end sequencing and 60 M total reads. Raw FASTQ files were processed using the nf-core RNAseq pipeline (nf-core/rnaseq v3.12.0) [40, 41]. Adapter and quality trimming was performed using Trim Galore v0.6.7 [42]. FASTQ reads were aligned to the mouse GRCm39 reference genome using STAR [43]. RNA sequencing transcripts were quantified using Salmon v1.10.1 [44]. Quantified transcripts were analyzed using the nf-core differential abundance pipeline (nf-core/differentialabundance v1.4.0) [40, 41]. Differential expression analysis was performed using DESeq2 v1.34.0 and EnhancedVolcano v1.20.0 from Bioconductor in R. GSEA v4.3.2 was used for gene set enrichment analysis [45]. Gene expression plots were made using ggplot2 in R [46].

Cell culture

MCF7 (HTB-22; ATCC) were cultured in Dulbecco's modified Eagle's medium (DMEM; D5796; Sigma Aldrich) supplemented with 10% foetal bovine serum (FBS; F1051; Sigma Aldrich) and 1% P/S at 37 °C and 5% CO_2. MCF7 and primary MECs were lentivirally infected in serum and antibiotic free medium containing 8 μg/mL polybrene. The pEIZ plasmid was a kind gift from Dr. B. Welm, and the pEIZ-Flag-Spy1 vector was generated as previously described [28]. The pLKO, pLKO-Spy1.1, pLKO-shSpy1.2, and pLB, pLB-shSpy1 plasmids were generated as described [16, 28]. The p53-GFP backbone was purchased from Addgene (11,770) (p53-GFP was a gift from Geoff Wahl (Addgene plasmid #11,770)), shp53 pLKO.1 puro was purchased from Addgene (19,119) (shp53 pLKO.1 puro was a gift from Bob Weinberg (Addgene plasmid # 19,119 ; http://n2t.net/addgene:19119 ; RRID: Addgene_19119)) [47].

Statistics

A Mann-Whitney was performed for tumour studies. For all other data, a Student's T-Test was performed. For experiments involving mouse samples and primary MECs, unequal variance was assumed. For cell line-based experiments, equal variance was assumed. For differential expression analysis, DESeq2 calculates *p*-values using the Wald test and BH-adjusted *p*-value (padj) is calculated using the Benjamini Hochberg method [48]. All experiments include at least 3 biological replicates and are representative of at least 3 experimental replicates.

Results

Spy1 increases ductal branching

The MMTV-Spy1 transgenic mouse model previously generated on a B6CBAF1/J background did not have any gross morphological differences in mammary development, despite changes in proliferation and apoptosis and a significant increase in mammary tumour susceptibility [20]. This was likely due to the nature of the model background as this strain is known to be more resistant to alterations in mammary development [49, 50]. To address this, the MMTV-Spy1 model was backcrossed 10 generations onto an FVBN/J background, a more commonly used strain for studying mammary development. Levels of Spy1 mRNA and protein were confirmed to be significantly upregulated in MMTV-Spy1 mice as compared to littermate controls (Figure S1 A, B). Previous data has demonstrated that elevation of Spy1 in HC11 cells was able to promote accelerated ductal development upon mammary fat pad transplantation [15]. Rate of ductal elongation and number of branch points was quantified throughout pubertal development. MMTV-Spy1 mice had a significant increase in ductal elongation at 8 weeks (Fig. 1A) and a significant increase in number of branch points across all time points collected (Fig. 1B: upper graph). A significant increase in the overall percent fat pad filling at all time points was also observed (Fig. 1B: lower graph). These alterations in ductal branching corresponded to a significant increase in the percentage of PCNA positive cells at all time points examined, and a significant decrease in cleaved caspase 3 (CC3) at 8 weeks of age (Figure S2A, B). Thus, Spy1 significantly increases rates of proliferation and decreases apoptosis at select time points in the developing mouse mammary gland. This may be a contributing factor to the increased ductal branching noted.

Increased rates of proliferation may impact the cellular composition of the mammary gland by altering cell cycle dynamics leading to changes in the differentiation status of the cells. First, inguinal mammary glands from 8-week-old mice were assessed for luminal and myoepithelial markers **c**yto**k**eratin **8** (CK8) and **s**mooth **m**uscle **a**ctin (SMA) respectively. No change in expression of either marker was noted in the MMTV-Spy1 inguinal mammary glands (Figure S2C). Hormone receptor status was assessed via immunohistochemistry from 8 and 12-week-old MMTV-Spy1 mice and littermate controls. MMTV-Spy1 mice showed accelerated expression of **p**rogesterone **r**eceptor (PR) and ERα positive cells at 8 weeks of age (Figure S3A-B). Previous work has demonstrated a feedback loop between Spy1 and p53 in the mammary gland [20]. Overall levels of p53 protein and RNA were assessed in 8-week-old MMTV-Spy1 and littermate control mice to determine if the developmental changes may be due to changes in p53 expression. No significant
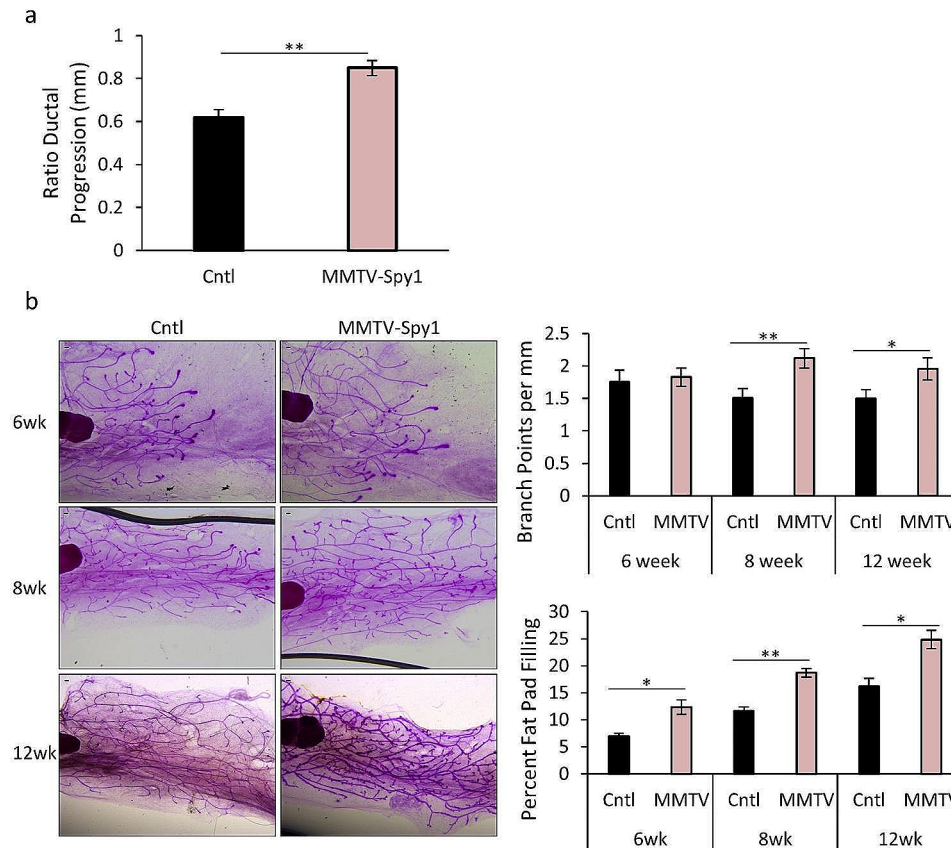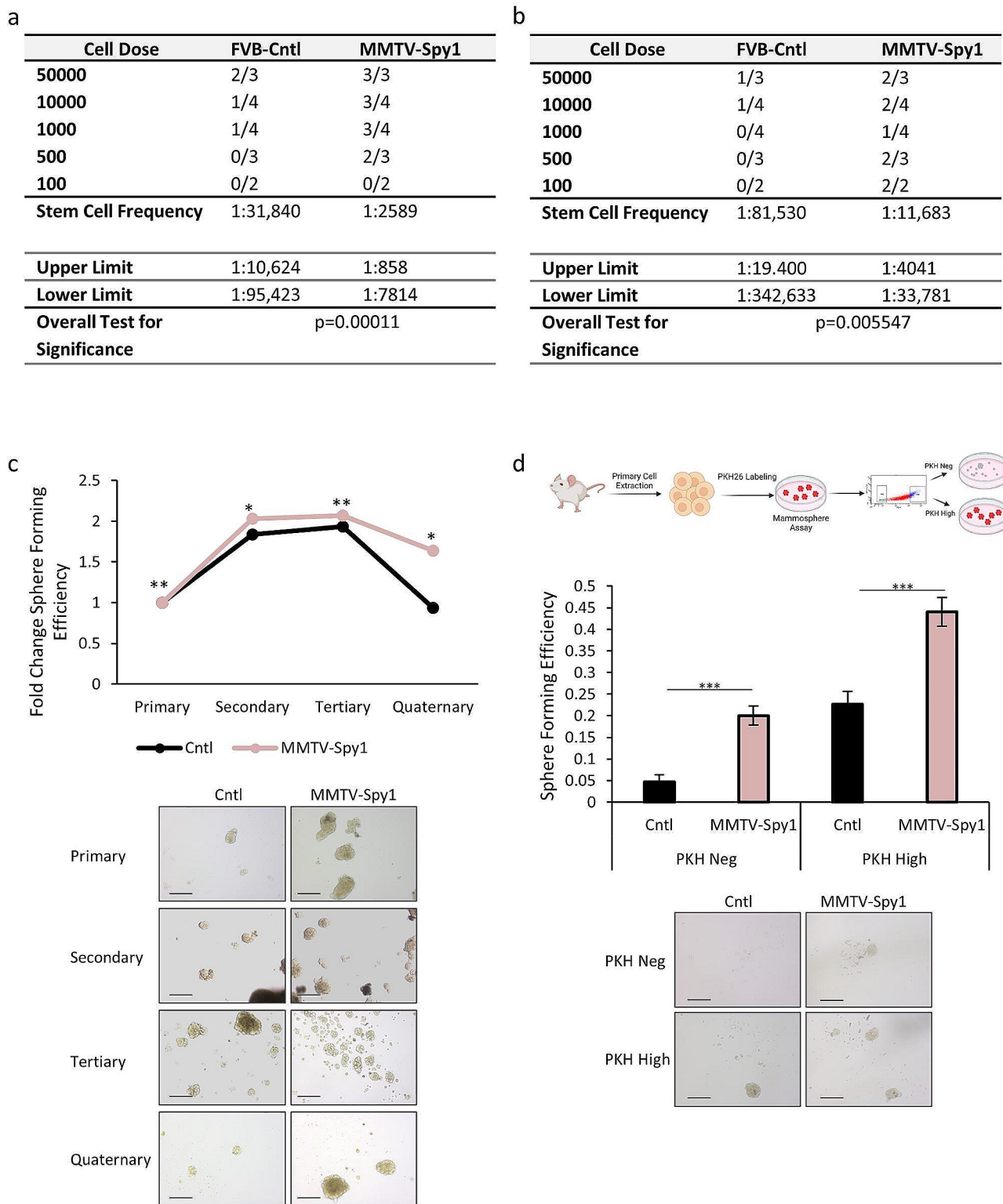
Fig. 1 Spy1 increases ductal branching. (**a**) Ratio of ductal progression past the lymph node in 8-week-old inguinal mammary glands from control littermates (Cntl) and MMTV-Spy1 mice ($n = 3$). (**b**) Whole mount analysis of inguinal mammary glands from 6-, 8- and 12-week-old littermate control and MMTV-Spy1 mice. Representative images shown in left panels, and quantification of number of branch points per mm (top right panel) and percentage of fat pad filling (bottom right panel) were quantified using ImageJ software analysis. Scale bar = 0.1 mm. (6-week $n = 4$-, 8- and 12-week $n = 3$); Errors bars represent SE; Student's T-test. *$p < 0.05$, **$p < 0.01$, ***$p < 0.001$

changes in p53 expression were detected (Figure S3C-D). This collectively supports that there is an early expansion of the hormone receptor positive population in mammary glands with Spy1 elevation, and potential alterations in the differentiation status of the mammary gland.

Elevated levels of Spy1 lead to expansion of the mammary stem cell population

An increase in proliferation coupled with alterations to the hormone receptor status in the mammary gland may impact the MaSC population, as this population is hormone receptor negative [51, 52]. To determine if Spy1 can promote expansion of the MaSC population, a limiting dilution assay was performed to assess functional properties of MaSCs using **m**ammary **e**pithelial **c**ells (MECs) isolated from 8-week-old mice to match time points collected during pubertal development. Strikingly, the MMTV-Spy1 mice had more than a 10-fold increase in the stem cell population (Fig. 2A). This increase was maintained over time as demonstrated using limiting dilution assays on MECs isolated from 6-month-old mice (Fig. 2B). As a secondary measurement of functional

properties of the stem cell population, primary MECs were isolated from 10-12-week-old MMTV-Spy1 mice and their control littermates and a mammosphere formation assay was performed. MECs isolated from MMTV-Spy1 mice had a significantly higher **s**phere **f**ormation **e**fficiency (SFE) as compared to control MECs when assessing the formation of primary spheres (Fig. 2C). Furthermore, a higher rate of SFE was sustained when sequentially passaged, whereas mammospheres from littermate controls demonstrated a decline in SFE over time (Fig. 2C). To further address the ability of Spy1 to promote stem cell characteristics in the mammary gland, primary MECs from MMTV-Spy1 and littermate control mice were isolated, stained with the label retaining dye PKH26 and seeded for a mammosphere formation assay. PKH26 is a fluorescent dye which binds cell membranes and segregates into daughter cells such that it can be used to identify proliferative history. It has been previously shown that mammary cells which retain high PKH26 staining contain a higher proportion of MaSCs as compared to PKH26 negative cells [11, 13, 53]. Following mammosphere formation, cells were sorted based on

a

Cell Dose	FVB-Cntl	MMTV-Spy1
50000	2/3	3/3
10000	1/4	3/4
1000	1/4	3/4
500	0/3	2/3
100	0/2	0/2
Stem Cell Frequency	1:31,840	1:2589
Upper Limit	1:10,624	1:858
Lower Limit	1:95,423	1:7814
Overall Test for Significance	p=0.00011	

b

Cell Dose	FVB-Cntl	MMTV-Spy1
50000	1/3	2/3
10000	1/4	2/4
1000	0/4	1/4
500	0/3	2/3
100	0/2	2/2
Stem Cell Frequency	1:81,530	1:11,683
Upper Limit	1:19.400	1:4041
Lower Limit	1:342,633	1:33,781
Overall Test for Significance	p=0.005547	

Fig. 2 MMTV-Spy1 mice have an increased MaSC population. Limiting dilution assays were performed using primary cells from (**a**) 8-week-old and (**b**) 6-month-old littermate control (FVB-Cntl) and MMTV-Spy1 mice. (**c**) Mammospheres from MMTV-Spy1 and littermate control mammary primary cells were serially passaged. Fold change in sphere forming efficiency is depicted (top panel; $n=3$). Representative images depicted in bottom panel. (**d**) Primary cells were isolated from control and MMTV-Spy1 inguinal mammary glands, stained with PKH26 and cultured and sorted as depicted in schema in top panel. Sphere forming efficiency is graphically represented in middle panel. Representative images depicted in bottom panel. ($n=6$); Scale bar $=200\ \mu m$; Errors bars represent SE; Student's T-test. *$p<0.05$, **$p<0.01$, ***$p<0.001$
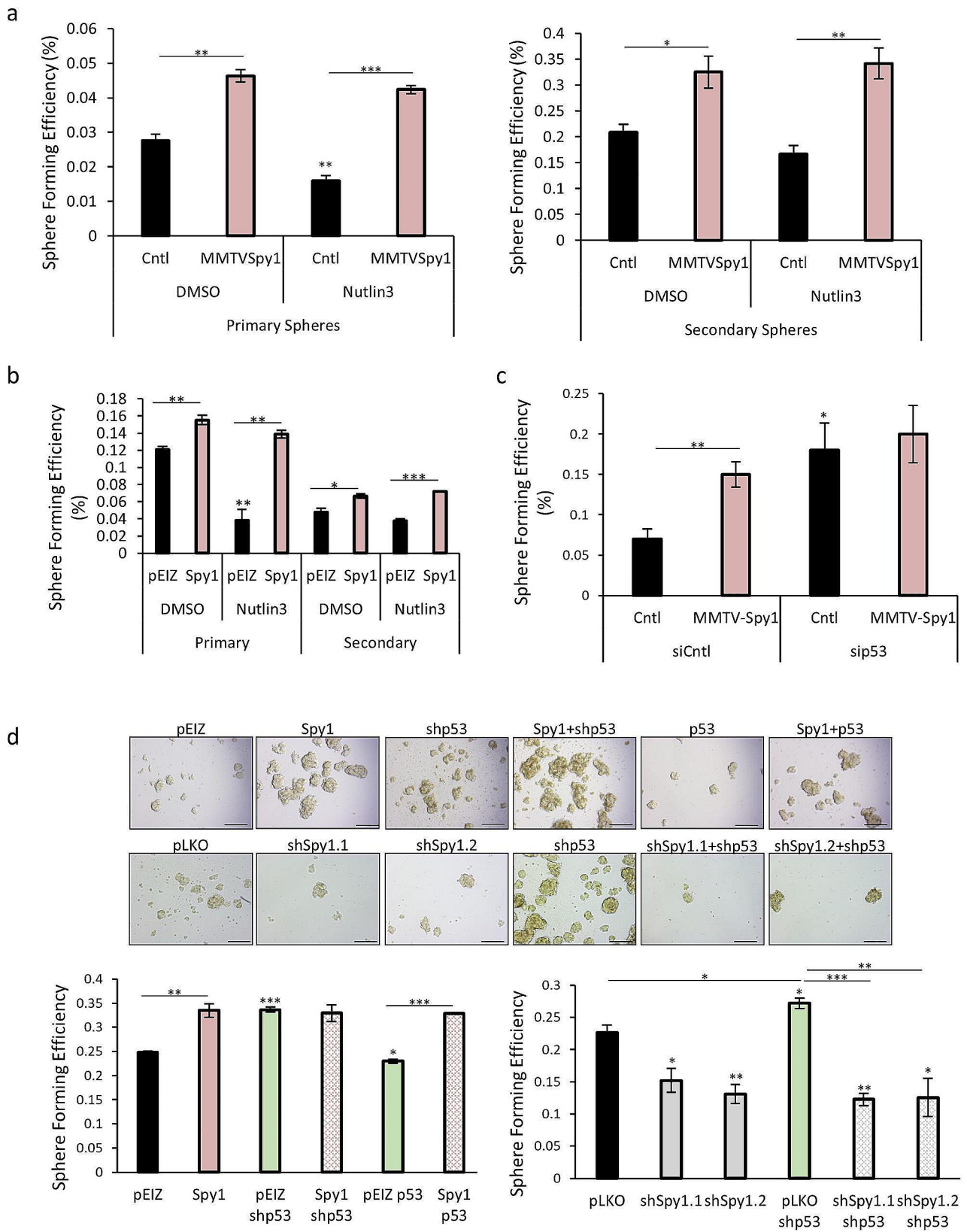
Fig. 3 (See legend on next page.)

(See figure on previous page.)

Fig. 3 Spy1 overrides p53 to promote MaSC expansion. (**a**) Primary mammary epithelial cells were isolated from inguinal mammary glands of MMTV-Spy1 and littermate control mice and cultured as mammospheres in the presence and absence of 2.5μM Nutlin3. Sphere forming efficiency of primary mammospheres (left panel) and secondary mammospheres (right panel) is depicted (*n* = 3). (**b**) Control (pEIZ) or Spy1 overexpression (Spy1) MCF7 cells were treated with 2.5μM Nutlin3 and cultured as mammospheres. Sphere forming efficiency in the presence or absence of Nutlin3 is depicted. (**c**) siRNA mediated knockdown of p53 was performed in primary mammary epithelial cells from control and MMTV-Spy1 inguinal mammary glands, and cells were cultured as mammospheres. Sphere forming efficiency is depicted (*n* = 5). (**d**) MCF7 cells were lentivirally infected with pEIZ, pEIZ Spy1 (Spy1), pLKO, pLKO shSpy1 (shSpy1.1, shSpy1.2), p53 or shp53. MCF7 cells with Spy1 overexpression (left panel) or Spy1 knockdown (right panels) in the presence or absence of p53, were cultured as mammospheres. Sphere forming efficiency was assessed and quantified (lower panels). Representative images shown in upper panels. Scale bar = 200 μm; *n* = 3; Errors bars represent SE; Student's T-test. *$p < 0.05$, **$p < 0.01$, ***$p < 0.001$

PKH26 staining and seeded as secondary mammospheres as PKH26^{high} and PKH26[negative] populations (Fig. 2D). As expected, PKH26[negative] populations had a reduced SFE compared to PKH26^{high} populations, however MMTV-Spy1 mammospheres increased SFE significantly in both PKH26[negative] and PKH26^{high} populations. Increased SFE in MMTV-Spy1 PKH26[negative] cell populations is indicative of increased functional properties of stemness in a population known to have reduced stem cell potential as has been previously demonstrated [13]. Taken together, this suggests that elevated levels of Spy1 promote stem cell potential of MECs, leading to expansion of the MaSC population.

Spy1 overrides p53 to promote expansion of the MaSC population

Spy1 can cooperate with the loss of p53 to promote susceptibility to mammary tumourigenesis, and functionally overrides p53 in response to various types of DNA damage [20, 24, 25]. Loss of p53 on its own leads to an increase in symmetric division and expansion of MaSC populations [11–14]. On the other hand, elevation of p53 supports a reduction in the MaSC population, asymmetric division and an increase in differentiation [11–13]. To determine if Spy1 plays a role in p53-mediated effects in the MaSC population, primary MECS from MMTV-Spy1 and littermate control mice were cultured as mammospheres in the presence and absence of Nutlin3, a small molecule that inhibits MDM2 dependent degradation of p53 leading to p53 stabilization [54]. SFE in control mammospheres was significantly reduced in the presence of Nutlin3 whereas no effect was seen on MMTV-Spy1 mammospheres (Fig. 3A), thus indicating that Spy1 can override p53 to allow for continued expansion of the MaSC population. This effect was also seen in MCF7 cells manipulated with lentivirus to overexpress Spy1 (Fig. 3B).

To assess the effects of loss of p53 in Spy1 overexpressing samples, primary MECs were again isolated from MMTV-Spy1 and littermate control mice and p53 was knocked down via siRNA and cells were seeded for mammosphere formation. As expected, knockdown of p53 increases SFE, however, while MMTV-Spy1 alone increased SFE, the combination of MMTV-Spy1 with sip53 did not result in a significant increase in SFE over that of sip53 alone (Fig. 3C). This suggests that Spy1

effects on MaSC expansion are via the ability to override p53. To further validate this result, MCF7 cells were manipulated with lentivirus to overexpress and knockdown both Spy1 and p53 in varying combinations. Spy1 was able to promote SFE in the presence of elevated p53 (Fig. 3D) and was not able to significantly increase SFE with loss of p53 (shp53) over that of shp53 alone (Fig. 3D). Interestingly, knockdown of Spy1 alone lead to a significant decrease in SFE and when combined with knockdown of p53, completely ablated the effects of loss of p53 on SFE indicating that in MaSCs with loss of p53, the ability to expand this population may be dependent on Spy1 (Fig. 3D). Taken together this data demonstrates that Spy1 can override p53 to promote MaSC expansion and may be required for promoting MaSC division with loss of p53.

Loss of p53 does not alter Spy1 mediated effects on normal mammary development

Despite alterations to ductal branching, early increases in hormone receptor positive cells and an increase in functional properties of stemness, only 2 spontaneous mammary tumours were documented over 50 MMTV-Spy1 mice allowed to age up to 2 years of age. Previous data has shown that Spy1 cooperates with loss of p53 to promote mammary tumourigenesis; however, whether the changes observed with Spy1 elevation during development, particularly with the MaSC population, contribute to increased susceptibility on a p53 null background has not yet been explored. To address this, MMTV-Spy1 mice were intercrossed with p53 null mice. First, inguinal mammary glands were collected at 8 weeks to determine if the loss of p53 altered any of the developmental phenotypes noted in the MMTV-Spy1 model. While there was a reduction in ductal elongation in the MMTV-Spy1 p53 heterozygous mice as compared to MMTV-Spy1 mice alone, the complete loss of p53 did not affect the ability of Spy1 to promote ductal elongation or increase the number of branch points, and rates of ductal elongation and branch points remained elevated over that of control mice and p53 heterozygous mice (Figure S4). No changes in differentiation status were observed with CK8 and SMA when assessing MMTV-Spy1 mice as compared to MMTV-Spy1 mice with partial or complete loss of p53 (data not shown). Previous work has characterized

a positive feedback loop between ERα and p53 [55, 56]. Additionally, there was no change on the ability of Spy1 to increase PR or ERα expression at 8 weeks in the absence of p53 (Figure S5A-B). Interestingly, p53 null mice had a significant increase in PR positive cells as compared to p53 heterozygous mice, however there was no significant difference in the presence of the MMTV-Spy1 transgene (Figure S5B). Collectively, these data support that Spy1 effects on mammary development are independent of p53 status.

To assess the cellular composition of the ductal network in the MMTV-Spy1 and p53 null intercrossed mice, flow cytometry was performed on MECs isolated from inguinal mammary glands of 8-week-old mice. While no significant differences were found between control, MMTV-Spy1, p53 heterozygotes and p53 null mice, MMTV-Spy1 mice with partial or complete loss of p53 both showed significant expansion of the luminal cell population (Figure S5C). MMTV-Spy1 p53 null glands also had a significant decrease in the basal cell population as compared to wildtype littermate controls (Figure S5C). This data supports that elevation of Spy1 combined with alterations in p53 status may alter the cellular composition of the mammary gland.

Spy1 p53 null tumours have elevated stem cell and cell cycle signaling

While loss of p53 did not alter ductal development or differentiation status of the mammary gland in combination with elevated Spy1, Spy1 and p53 do appear to have a link with respect to the MaSC population. To address the impact of increased stemness properties on Spy1 p53 null driven tumours, MMTV-Spy1 mice were again intercrossed with p53 null mice. Primary MECs were extracted at 8 weeks of age and mammary fat pad transplantation was performed in cleared glands of 3-week-old FVBN/J mice as described to eliminate the potential of other tumours arising on a p53 null background prior to mammary tumours developing [20]. Similar to previous findings, Spy1 cooperated with partial or complete loss of p53 to increase hyperplastic alveolar nodules (HANs) and tumour formation (Fig. 4A). MMTV-Spy1 p53 null mice had a significant increase in both HANs and tumour formation over that of control mice, and p53 null and MMTV-Spy1 p53 heterozygous mice displayed significant increases in HANs formation over that of control mice. When comparing rates of both HANs and tumour formation between p53 altered genotypes with and without Spy1 elevation, no significant differences were noted despite an increasing trend in incidence rates (Fig. 4A). No significant difference in rate of tumour onset was found (Figure S6A). Immunohistochemical analysis revealed a significant increase in the percentage of phospho-histone H3 positive cells in all tumours with

Spy1 elevation as compared to p53 heterozygous and p53 null tumours alone (Fig. 4B). p53 null tumours had the highest percentage of CC3 positive cells and a significant decrease in CC3 positive cells was seen in Spy1, Spy1 p53 heterozygous and Spy1 p53 null tumours as compared to p53 null alone (Fig. 4C). Interestingly, p53 heterozygous tumours had the lowest amount of CC3 positive cells with Spy1 p53 heterozygous and Spy1 p53 null tumours having significantly increased rates of apoptosis over p53 heterozygous alone (Fig. 4C). p53 expression levels were confirmed to be significantly reduced as compared to control mammary gland tissue via qRT-PCR (Figure S6B) and western blot analysis (data not shown) with no significant differences when taking into consideration the presence of the MMTV-Spy1 transgene. Taken together, this data demonstrates that Spy1 elevation alone or in combination with partial or complete loss of p53 increases rates of proliferation and decreases apoptosis as compared to p53 null tumours (Fig. 4B-C).

Histological analysis revealed that the Spy1, p53 null and Spy1 p53 null tumours shared close histological features within groups rather than shared features between groups (Figure S6C), suggesting differences in tumour subtypes and cellular composition. Differences in histology may point to alterations in key signaling pathways between p53 null and Spy1 p53 null driven tumours. To further elucidate these differences, RNA sequencing (RNAseq) followed by **G**ene **S**et **E**nrichment **A**nalysis (GSEA) [45] was performed on p53 null and Spy1 p53 null tumours. GSEA revealed upregulation of pathways associated with branching in mammary gland duct morphogenesis, as well as elevated breast cancer and mammary luminal progenitor pathways (Fig. 5, S7, S8). Pathways associated with breast cancer progression and increased cell cycle signaling were also upregulated (Fig. 5, S7-S9). Thus, this analysis revealed commonalities in upregulated signaling pathways associated with changes observed in the normal mammary gland that may be contributing factors to susceptibility to tumourigenesis.

When assessing changes in gene expression, approximately 500 genes were significantly upregulated while over 600 genes were significantly downregulated in Spy1 p53 null tumours as compared to p53 null alone (Fig. 6A). Among the top genes significantly upregulated was Chi3l1 (Chil1) (Fig. 6B), a gene associated with poor prognosis in breast cancer [57]. In addition, other genes associated with stem cell populations or changes seen in MMTV-Spy1 mice during normal mammary development were also impacted. FoxA1, a known driver of stem cell proliferation and regulator of ERα expression [58], as well Prom1, a regulator of luminal cell differentiation and ductal branching [59] were also significantly upregulated (Fig. 6C, D). Significantly downregulated was Cdkn1a, a
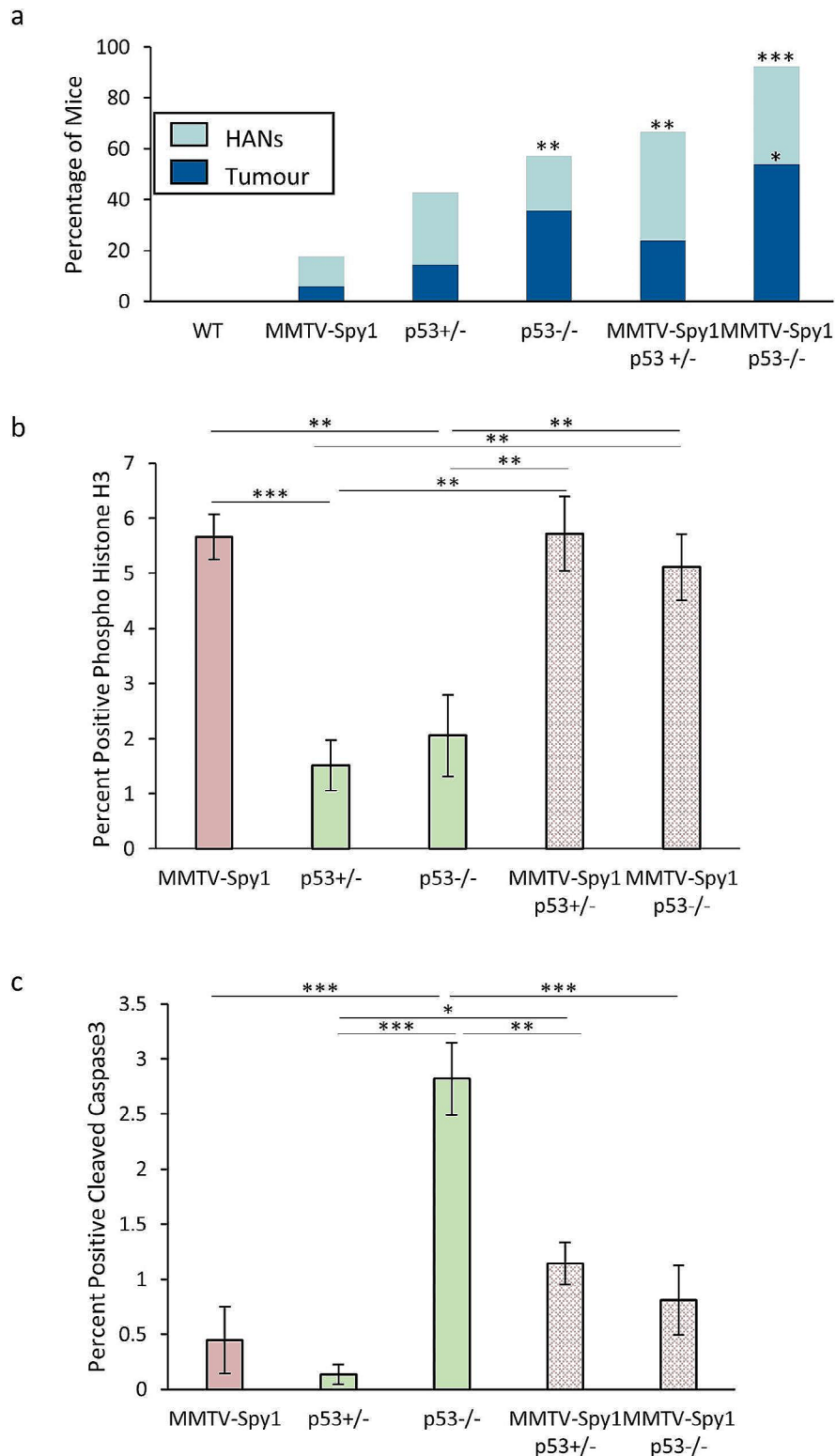
Fig. 4 Elevated Spy1 increases mammary tumour formation. (**a**) Primary mammary epithelial cells from MMTV-Spy1 and p53 null intercrossed mice were injected into the cleared fat pads of wildtype mice and monitored weekly for HANs and tumour development. HANs were only quantified in tumour negative mice (Cntl *n* = 15, MMTV-Spy1 *n* = 17, p53+/- *n* = 21, p53-/- *n* = 14, MMTV-Spy1 p53+/- *n* = 21, MMTV-Spy1 p53-/- *n* = 13). Immunohistochemical analysis of (**b**) phospho histone H3 and (**c**) cleaved caspase 3 in Spy1 p53 null and p53 null tumours (p53 null *n* = 3; Spy1 p53 null *n* = 4). Quantification of percent positive (**b**) phospho histone H3 or (**c**) cleaved caspase 3 depicted graphically. Scale bar = 100 μm; Mann-Whitney (**a**) and Student's T-test (b&c). *$p < 0.05$, **$p < 0.01$, ***$p < 0.001$
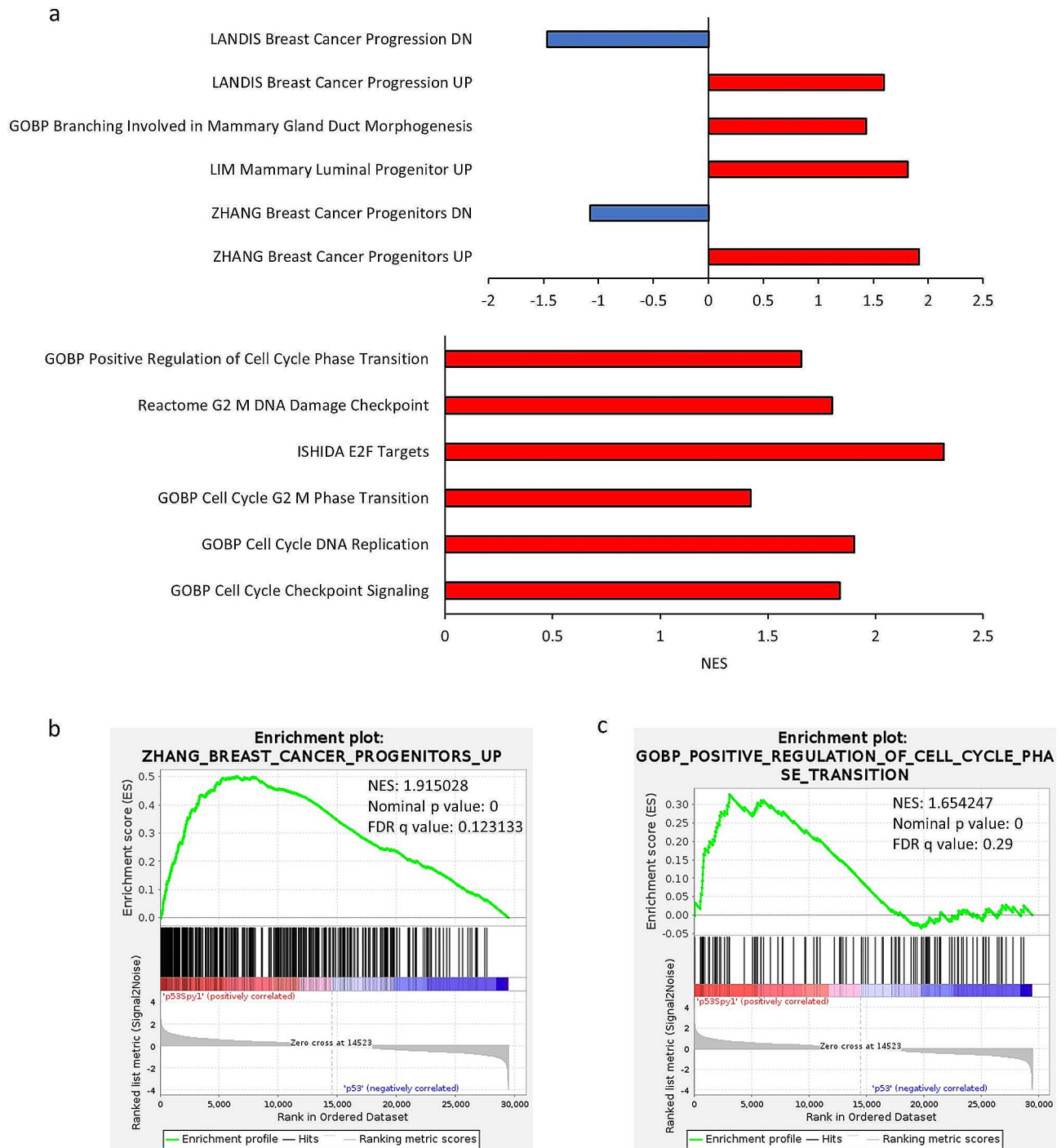
Fig. 5 Spy1 driven tumours have unique signaling pattern. GSEA was performed on Spy1 p53 null versus p53 null driven tumours. (**a**) Normalized enrichment scores (NES) of selected gene sets are depicted graphically. (**b**) Enrichment plots of breast cancer progenitor gene set (left panel) and positive regulation of cell cycle phase transition gene set (right panel) are depicted

target of p53 and inhibitor of MaSC expansion (Fig. 6E). To validate these findings, expression of Chi3l1, FoxA1, Prom1 and Cdkn1A were examined via qRT-PCR in Spy1 p53 null and p53 null tumours as well as MMTV-Spy1 p53 null intercrossed inguinal mammary glands from 8-week-old mice (Figure S10). qRT-PCR analysis of

tumour samples confirmed the findings from RNAseq, and similar trends were seen in p53 null and MMTV-Spy1 p53 null 8-week-old inguinal mammary glands (Figure S10), thus demonstrating that early changes in normal development may contribute to the onset of tumourigenesis and tumour characteristics.
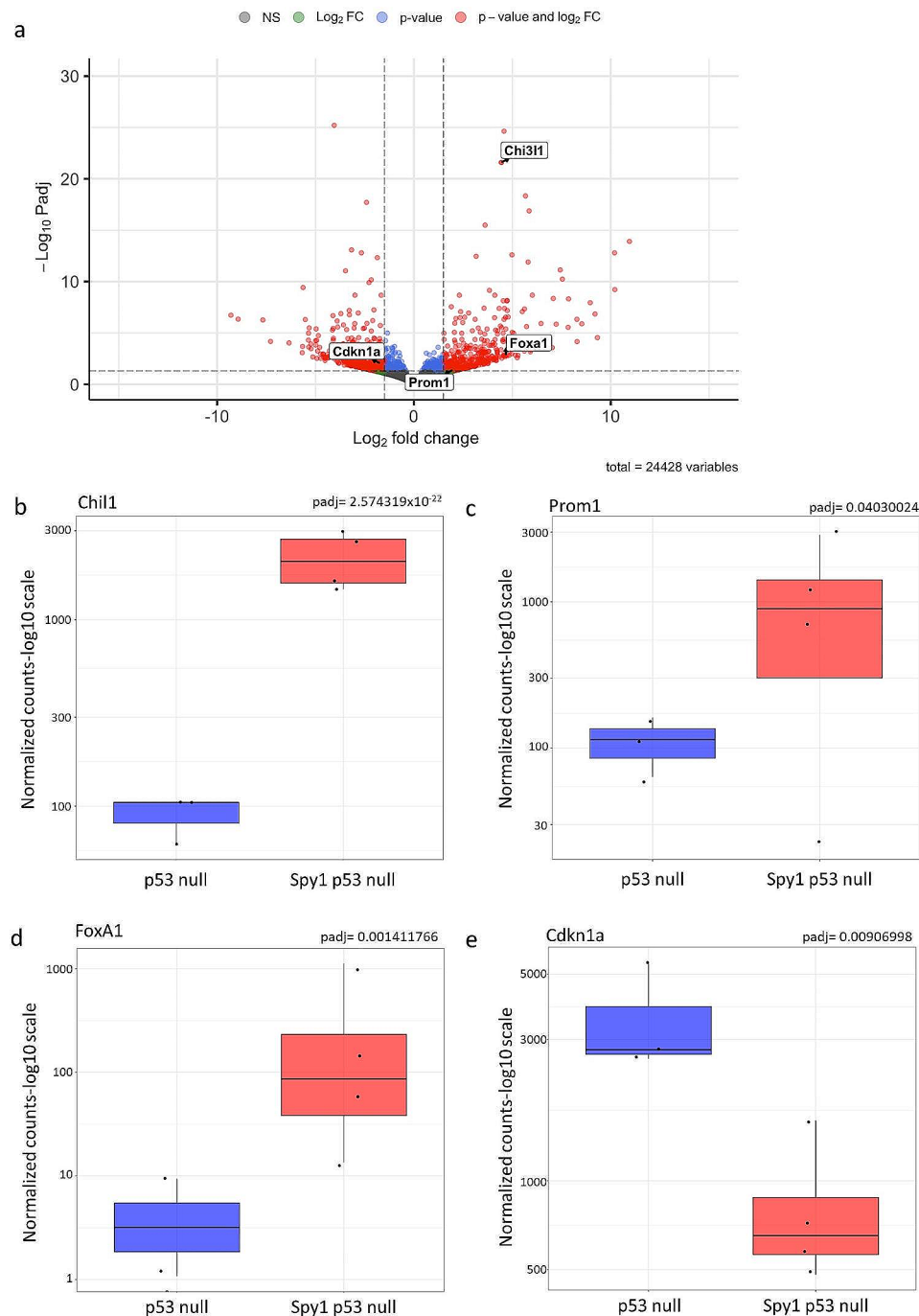
Fig. 6 Changes in gene expression reflect gene set and developmental changes with elevated Spy1 expression. (**a**) Volcano plot depicting differentially expressed genes in Spy1 p53 null as compared to p53 null tumours. Normalized gene expression counts of (**b**) Chil1 (Chi3l1), (**c**) Prom1, (**d**) FoxA1 and (**e**) Cdkn1a from RNA sequencing data with BH-adjusted *p*-value from DESeq2 indicated in the top right of each graph

Expansion of the breast cancer stem cell population with loss of p53 and elevated Spy1 drives therapeutic resistance

Given the changes in signaling pathways associated with stem cell populations seen in Spy1 p53 null tumours, the stem cell population was assessed to determine if tumours arising in glands with elevated Spy1 had an increased proportion of stem cells. Primary tumour cells were isolated and cultured in non-adherent conditions to test SFE. When comparing cells from p53 null and MMTV-Spy1 p53 null tumours, a significantly higher SFE was found in the MMTV-Spy1 p53 null tumours as compared to p53 null tumours alone (Fig. 7A). A higher rate of SFE was seen when examining secondary sphere formation, although this effect was not significant (Fig. 7A).

Fifield *et al. Breast Cancer Research*   (2024) 26:106

Page 13 of 18
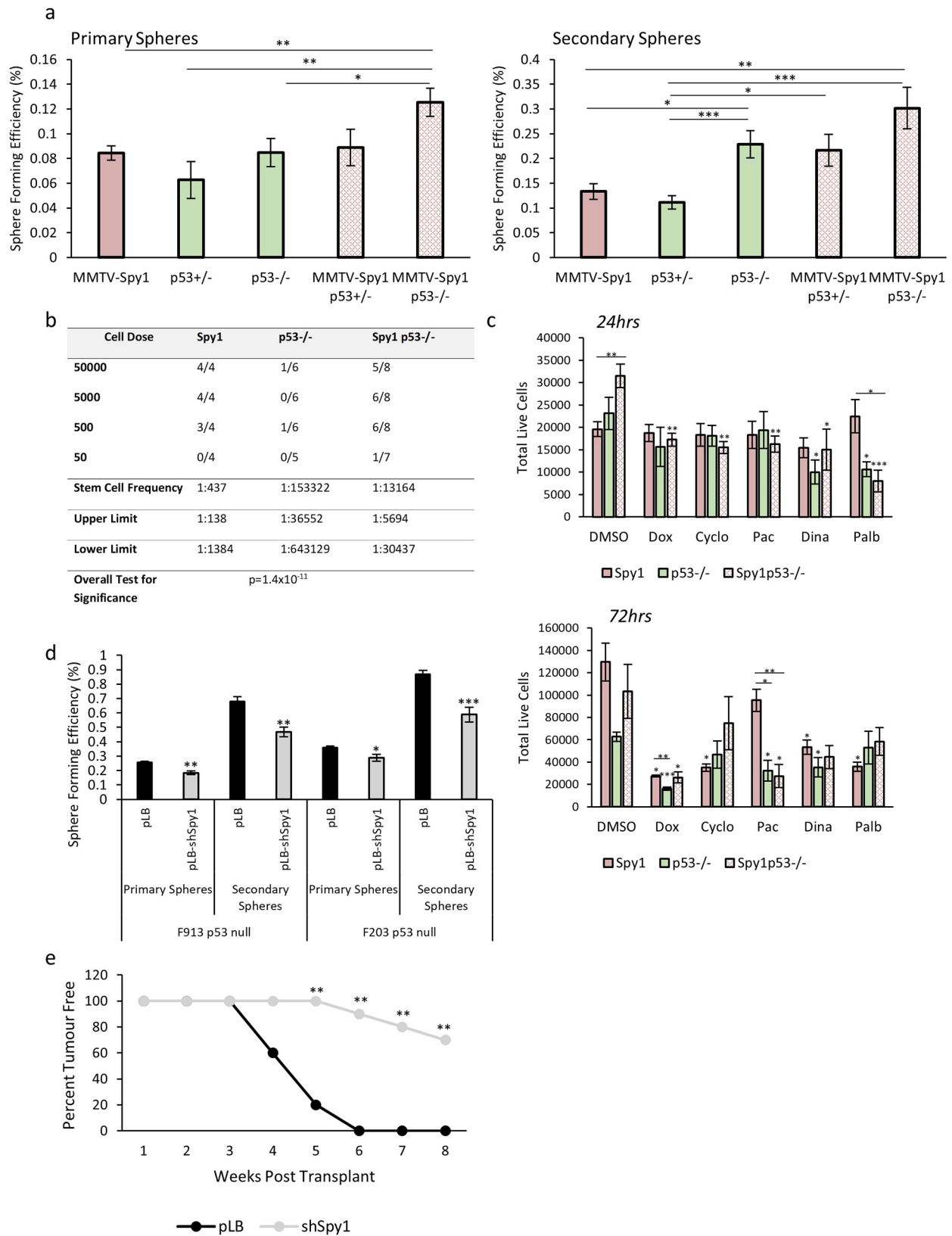
Fig. 7 (See legend on next page.)

(See figure on previous page.)

Fig. 7 Loss of Spy1 delays tumour onset. (**a**) Cells were isolated from tumours developed following mammary fat pad transplantation and mammosphere formation assays were performed. Sphere forming efficiency was quantified in primary (left panel) and secondary (right panel) mammospheres ($n = 3$). (**b**) Primary cells from Spy1, p53 null and Spy1 p53 null tumours were injected into fat pads of wildtype mice for a limiting dilution assay. (**c**) Primary tumour cells from Spy1, p53 null and Spy1 p53 null tumours were treated with a panel of therapeutic agents for 24 h (top panel) and 72 h (bottom panel). Trypan blue exclusion analysis was performed to assess total number of live cells ($n = 3$). (**d**) Primary cells from p53 null tumours were infected with lentivirus containing control (pLB) or Spy1 knockdown (pLB-shSpy1) and cultured as mammospheres. Sphere forming efficiency was assessed and quantified for primary and secondary spheres ($n = 3$). (**e**) p53 null primary tumour cells infected with control (pLB) or knockdown of Spy1 (pLB-Spy1) were injected into fat pad of FVBN/J mice. Timing of tumour onset is depicted ($n = 10$). Errors bars represent SE; Student's T-test (**a**, **c, d**), Mann-Whitney (**e**). *$p < 0.05$, **$p < 0.01$, ***$p < 0.001$. Single asterisks over bar indicates significance to DMSO within genotype in panel c)

MMTV-Spy1 p53 heterozygous primary tumour cells had comparable SFE to p53 null tumour cells in both primary and secondary sphere formation assays, and MMTV-Spy1 p53 null primary and secondary spheres had the highest SFE across all genotypes of primary tumour cells examined correlating with the highest incidence of HANs and tumour formation (Fig. 7A). In addition, mammospheres from Spy1 tumours were significantly larger than mammospheres from any tumours with p53 alteration (Figure S11). A limiting dilution assay was performed on primary tumour cells from Spy1, p53 null and Spy1 p53 null tumours as a gold standard test of functional stem cell properties to the observed increase in the **b**reast **c**ancer **s**tem **c**ell (BCSC) population. p53 null tumours had the lowest population of BCSCs as compared to Spy1 alone and Spy1 p53 null tumours (Fig. 7B). Taken together, this data demonstrates that Spy1 leads to expansion of not only the normal MaSC population, but also the BCSC population.

Spy1 driven tumours have a significant increase in the BCSC population, and increased cell cycle progression signaling. The BCSC population is hypothesized to be a driving force in driving breast tumour growth and relapse [10], due in part to drug resistance, and this combined with alterations in cell cycle progression, may point to a role for Spy1 in driving drug resistance. To test this, primary tumour cells from Spy1, p53 null and Spy1 p53 null tumours were treated with a variety of chemotherapeutic agents and inhibitors that target various aspects of the cell cycle machinery for 24 and 72 h. While the trends for each agent used varies, in most cases those tumours with elevated Spy1 displayed increased cell viability to varying degrees following drug treatment over p53 null tumours alone (Fig. 7C).

### Loss of Spy1 delays tumour formation and decreases the BCSC population

To determine if Spy1 is essential for expanding the BCSC population in p53 null tumours, Spy1 was knocked down using lentiviral manipulation in two p53 null primary tumour cell lines. Manipulated cells were then seeded for mammosphere formation assays. A decrease in Spy1 levels resulted in a significant decrease in SFE in both primary tumour cell lines in both primary and secondary mammospheres (Fig. 7D). Next, control and Spy1

knockdown p53 null primary tumour cells were injected into inguinal mammary glands of 6-week-old mice and followed for tumour formation. The knockdown of Spy1 lead to a significant decrease in tumour formation as compared to control (Fig. 7E). Thus, Spy1 cooperates with loss of p53 to drive the initiation and progression of drug resistant breast tumours with an increased BCSC population, which may be a contributing factor to therapy resistance and relapse (Fig. 8).

Discussion

Disruptions during normal mammary development that alter the ductal network and cellular composition of the mammary gland can have long lasting implications including increased susceptibility to mammary tumourigenesis. The transgenic MMTV-Spy1 mouse model revealed that sustained elevation of Spy1 can promote susceptibility to breast tumourigenesis by altering normal ductal development and increasing the MaSC population, a vulnerable population of cells thought to be the cell of origin for many types of breast cancer [8, 9]. Overexpression of Spy1 within the mouse mammary gland leads to increased ductal branching and enhanced ductal elongation, in part due to increased proliferation. While common luminal and basal differentiation markers remain unaltered, Spy1 accelerated the expression of hormone receptors. Previous work has shown that Spy1 mediated activation of ERK signaling leads to a significant increase in ligand independent phosphorylation and activation of ERα [31]. Whether the increase in ERα seen in vivo is mediated through a similar mechanism is an important next step of investigation. Given the important role hormone receptor signaling plays in regulating MEC proliferation, alterations in hormone receptor status may have profound implications on proliferative status and mutational accumulation over the lifetime of the mammary gland. Thus, the alteration in hormone receptor status and proliferative state of the mammary glands of MMTV-Spy1 mice may create an environment primed for oncogenesis.

In addition to alterations in hormone receptor status, the MaSC population was significantly increased in MMTV-Spy1 mice. Elevated levels of Spy1 were able to impart stemness properties to cell populations known to have reduced stem cell potential and increased the
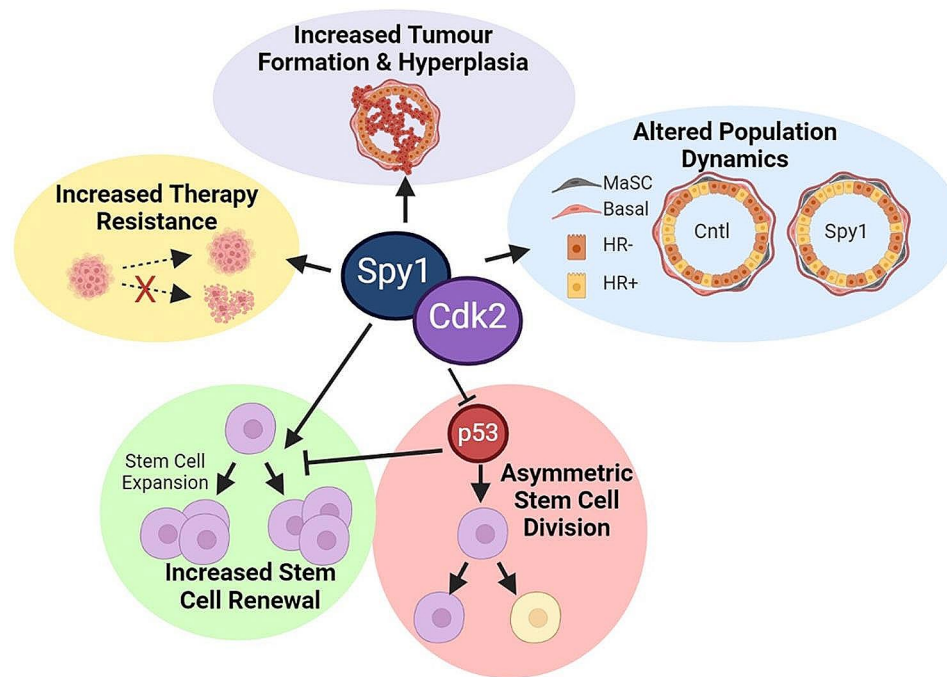
Fig. 8 Summary of effects of elevated Spy1 on normal and abnormal development of the breast. Elevated Spy1 drives expansion of the MaSC population, in part by overriding p53, leading to initiation of tumours with an increase in the BCSC population. Spy1 p53 null tumours have a unique signaling signature over that of p53 null tumours which in part may contribute to increased therapeutic resistance

frequency of the MaSC population as observed through functional assays assessing stem cell properties. MaSC populations are considered vulnerable cell populations to damaging events and may be the cell of origin for mammary tumourigenesis [8, 9]. Tumour suppressors such as p53 have tight control over expansion of this population, with p53 promoting asymmetric division, preventing dangerous expansion of this population [11]; however, Spy1 was able to override p53 and promote continued expansion of the MaSC population even in the presence of elevated p53. In addition, knockdown of p53 demonstrated that the enhanced stem cell expansion seen with loss of p53 requires Spy1 expression as the combined loss of Spy1 and p53 prevented continued expansion of the stem cell population. Further work is required to determine the exact mechanism by which this occurs and if Spy1 is expanding the MaSC population via alterations in asymmetric versus symmetric division, as has been seen in the brain tumour initiating cell population [28].

Further demonstrating the implications of an expanded MaSC population, the combined loss of Spy1 and p53 led to development of mammary tumours with an increased BCSC population and increased signaling associated with breast cancer progenitor populations. This demonstrates the critical role that maintenance of checkpoint signaling plays in restraining the MaSC population to prevent the expansion of a vulnerable cell population with potentially deleterious mutations that can act as the

cell of origin in mammary tumourigensis. Further work is needed to address whether MaSCs are truly the cell of origin in Spy1 mediated mammary tumourigenesis. Lineage tracing assays are a critical next step in assessing cell fate and cellular hierarchies to determine exactly which cell populations Spy1 is implicated in, and whether the MaSC population is driving Spy1 mediated tumour susceptibility. Tumours with elevated Spy1 had a significant increase in various mediators of breast cancer prognosis and normal mammary gland development that were also altered in samples obtained from MMTV-Spy1 p53 null intercrossed mice during puberty. Chi3l1 is associated with poor prognosis and has recently been shown to have a role in promoting an immunosuppressive tumour immune microenvironment in a mouse model of breast cancer [60]. Whether Spy1 may also be capable of contributing to an immunosuppressive state in mammary tumours is an important area of future study. Spy1 p53 null tumours also had a significant increase in FoxA1 and Prom1, both important mediators of normal mammary development and both implicated in BCSC populations [58, 59, 61, 62]. These changes in expression are linked to changes observed in mammary gland development of MMTV-Spy1 mice, as increased ductal branching and accelerated hormone receptor expression were observed and would be consistent with elevated FoxA1 and Prom1 expression [58, 59]. Importantly, Spy1 has previously been shown to expand Prom1 cancer stem cell

Fifield *et al. Breast Cancer Research*   (2024) 26:106

Page 16 of 18

populations in brain tumours [28]. Given the evidence to support the existence of a Prom1 positive BCSC population [62], exploring whether Spy1 is selectively mediating this population through similar changes in symmetric division seen in Prom1 positive brain tumour initiating cell populations is important future work [28].

Analysis of the tumours revealed an increase in cell cycle signaling in tumours with elevated Spy1 and loss of p53 as compared to loss of p53 alone. Spy1 p53 null tumours were more resistant to various forms of therapy and had increased proliferative and decreased apoptotic capacity. This increase in tumour cell cycle signaling highlights the important role intact cellular checkpoints play in maintaining the integrity of the cell, and points to a potential role for Spy1 in the early stages of the initiation of tumourigenesis via disruption of cellular checkpoints and altered proliferative status. Restoration of cellular checkpoints to inhibit cellular proliferation and promote apoptosis has long been a goal of therapeutic intervention. This data supports that Spy1 could be a novel therapeutic target for a select subset of breast cancer patients with elevated levels of Spy1.

Conclusions

Collectively, this data demonstrates that the atypical cell cycle regulator Spy1 plays an important role during normal mammary development. Overexpression of Spy1 alters the proliferative status of the mammary gland leading to acceleration of ductal elongation and increased ductal branching. Spy1 also alters the cellular composition of the mammary gland leading to altered hormone receptor status expression and expansion of the MaSC population. This data shows for the first time that the ability of Spy1 to override p53 can lead to changes in distinct cell populations with Spy1 able to override p53 driven asymmetric division of the MaSC population promoting increased expansion. This leads to increased susceptibility to mammary tumour formation with alterations in key checkpoint signaling pathways elucidating an important potential new therapeutic target for the treatment of select subsets of breast cancer patients.

Abbreviations

BCSC	Breast cancer stem cell
CC3	Cleaved caspase 3
Cdk	Cyclin dependent kinase
CK	Cytokeratin
ERα	Estrogen receptor alpha
HANs	Hyperplastic alveolar nodules
MaSC	Mammary stem cell
MEC	Mammary epithelial cell
PR	Progesterone receptor
SFE	Sphere forming efficiency
SMA	Smooth muscle actin

Supplementary Information

The online version contains supplementary material available at https://doi.org/10.1186/s13058-024-01862-1.

Supplementary Figure 1: Spy1 is overexpressed in MMTV-Spy1 mammary glands. (**a**) qRT-PCR analysis of inguinal mammary glands from MMTV-Spy1 and littermate controls (Cntl) for Spy1 levels corrected for GAPDH (n = 4). (**b**) Spy1 expression in inguinal mammary glands collected from 8-week-old MMTV-Spy1 and littermate control (Cntl) mice. Representative images in bottom panels with quantification of Spy1 levels using ImageJ software analysis shown in the top panel. Scale bar = 100 μm (n = 3). Errors bars represent SE; Student's T-test. *p < 0.05, **p < 0.01, ***p < 0.001

Supplementary Figure 2: Spy1 increases proliferation and decreases apoptosis. (**a**) PCNA expression in MMTV-Spy1 and littermate controls via immunohistochemical analysis. Quantification of percentage of PCNA positive mammary epithelial cells over five fields of view per sample. Scale bar = 100μM (**b**) Cleaved caspase-3 (CC3) expression in MMTV-Spy1 and littermate controls via immunohistochemical analysis. Quantification of percentage of CC3-positive mammary epithelial cells over five fields of view per sample. Scale bar = 100μM. (**c**) Representative images of immunohistochemical analysis of CK8 and SMA. Scale bar = 100μM. n = 3; Error bars represent SE; Student's T test. *p < 0.05, **p < 0.01, ***p < 0.001

Supplementary Figure 3: Altered hormone receptor status with elevated Spy1. Immunohistochemical analysis of (**a**) PR and (**b**) ER in 8- and 12-week-old MMTV-Spy1 and littermate control inguinal mammary glands. Representative images shown in left panels, where blue represents hematoxylin nuclear stain and brown represents (**a**) PR or (**b**) ER. Quantification of the percent positive (**a**) PR and (**b**) ER cells are depicted in right panels. Scale bar = 100 μm; (**c**) qRT-PCR analysis of inguinal mammary glands from control (cntl) and MMTV-Spy1 mice of p53 levels corrected for GAPDH. (**d**) Levels of p53 were assessed via western blot analysis in inguinal mammary glands of control (cntl) and MMTV-Spy1 mice. Left panel depicts densitometry analysis of p53 expression corrected for actin and right panel depicts representative blot. n = 3; Errors bars represent SE; Student's T-test. *p < 0.05, **p < 0.01, ***p < 0.001

Supplementary Figure 4: Loss of p53 does not alter Spy1 driven mammary development effects. Whole mount analysis was performed on inguinal mammary glands from 8 week old MMTV-Spy1 and p53 null intercrossed mice. (**a**) Ductal progression past lymph node and (**b**) number of branch points per mm of primary duct was quantified (Cntl n = 4, MMTV-Spy1 n = 5, p53+/- n = 5, p53-/- n = 4, MMTV-Spy1 p53+/- n = 7, MMTV-Spy1 p53-/- n = 3). Scale bar = 100μM. n = 3; Error bars represent SE; Student's T test. *p < 0.05, **p < 0.01, ***p < 0.001

Supplementary Figure 5: Loss of p53 does not alter hormone receptor expression in MMTV-Spy1 mice. Immunohistochemical analysis of the percent positive (**a**) ER and (**b**) PR in 8-week-old inguinal mammary glands of MMTV-Spy1 and p53 null intercrossed mice. Percent positive cells is represented graphically (Cntl n = 6, MMTV-Spy1 n = 7, p53+/- n = 4, p53-/- n = 3, MMTV-Spy1 p53+/- n = 6, MMTV-Spy1 p53-/- n = 3). (**c**) Flow cytometry analysis of primary mammary epithelial cells from inguinal glands of MMTV-Spy1 and p53 null 8-week-old intercrossed mice (Cntl n = 6, MMTV-Spy1 n = 8, p53+/- n = 6, p53-/- n = 3, MMTV-Spy1 p53+/- n = 8, MMTV-Spy1 p53-/- n = 4); Errors bars represent SE; Student's T-test. *p < 0.05, **p < 0.01, ***p < 0.001

Supplementary Figure 6: Primary mammary epithelial cells from MMTV-Spy1 and p53 null intercrossed mice were injected into the cleared fat pads of wildtype mice and monitored weekly for HANs and tumour development. (**a**) Timing of tumour onset is depicted. (**b**) qRT-PCR analysis of p53 levels corrected for GAPDH in Spy1, p53 null and Spy1 p53 null tumours (Spy1 n = 1; p53 null n = 3; Spy1 p53 null n = 3). (**c**) Representative hematoxylin and eosin stained images from Spy1, p53 null and Spy1 p53 null tumours. Scale bar = 100μM. (Cntl n = 15, MMTV-Spy1 n = 17, p53+/- n = 21, p53-/- n = 14, MMTV-Spy1 p53+/- n = 21, MMTV-Spy1 p53-/- n = 13)

Supplementary Figure 7: Dot plots depicting 2 sets of gene sets altered in Spy1 p53 null tumours as compared to p53 null tumours. Plots depict altered (**a**) breast specific gene sets and (**b**) cell cycle progression gene sets

Supplementary Figure 8: Spy1 driven tumours have enrichment in pro-

genitor and breast cancer progression signaling. GSEA demonstrated that Spy1 p53 null tumours are enriched in (**a**) mammary luminal progenitors, (**b**) branching morphogenesis, and (**c**) breast cancer progression gene sets and are depleted for genes downregulated in (**d**) breast cancer progenitors and (**e**) breast cancer progression

Supplementary Figure 9: Spy1 driven tumours are enriched in cell cycle progression gene sets. GSEA demonstrated that Spy1 p53 null driven tumours are enriched in (**a**) cell cycle checkpoint signaling, (**b**) cell cycle G2 M phase transition, (**c**) E2F targets, (**d**) G2 M DNA damage checkpoint, and (**e**) cell cycle DNA replication gene sets

Supplementary Figure 10: Changes in expression in Spy1 driven tumours are reflected during normal development. qRT-PCR analysis of expression of (**a**) Chi3l1, (**b**) Prom1, (**c**) FoxA1 and (**d**) Cdkn1a corrected for GAPDH in Spy1 p53 null and p53 null tumours (p53 null n = 3; Spy1 p53 null n = 5). qRT-PCR analysis of expression of (**e**) Chil3l1, (**f**) Prom1, (**g**) FoxA1 and (**h**) Cdkn1a corrected for GAPDH from inguinal mammary glands of 8 week old MMTV-Spy1 p53 null intercrossed mice (n = 3). Errors bars represent SE; Student's T-test. *p < 0.05, **p < 0.01

Supplementary Figure 11: (**a**) Primary tumour cells from MMTV-Spy1 and p53 null tumours were cultured as mammospheres. Sphere diameter of primary (left panel) and secondary (right panel) mammospheres was quantified. N = 3; Error bars represent SE; Student's T test. *p < 0.05, **p < 0.01, ***p < 0.001

Supplementary Figure 12: (**a**) Uncropped gel images from western blot images depicted in figure S3d

Data availability
Data is available upon request.

Declarations

Ethics approval and consent to participate
Mice were maintained following the Canadian Council on Animal Care guidelines under animal utilization protocol 20 – 15 approved by the University of Windsor.

Consent for publication
Not applicable.

Competing interests
The authors declare no competing interests.

References
1. Fantl V, Stamp G, Andrews A, Rosewell I, Dickson C. Mice lacking cyclin D1 are small and show defects in eye and mammary gland development. Genes Dev. 1995;9(19):2364–72.
2. Hennighausen L, Robinson GW. Signaling pathways in mammary gland development. Dev Cell. 2001;1(4):467–75.
3. Ray D, Terao Y, Christov K, Kaldis P, Kiyokawa H. Cdk2-null mice are resistant to ErbB-2-induced mammary tumorigenesis. Neoplasia. 2011;13(5):439–44.
4. Landis MW, Pawlyk BS, Li T, Sicinski P, Hinds PW. Cyclin D1-dependent kinase activity in murine development and mammary tumorigenesis. Cancer Cell. 2006;9(1):13–22.
5. Shehata M, Waterhouse PD, Casey AE, Fang H, Hazelwood L, Khokha R. Proliferative heterogeneity of murine epithelial cells in the adult mammary gland. Commun Biol. 2018;1:111.
6. Richert MM, Schwertfeger KL, Ryder JW, Anderson SM. An atlas of mouse mammary gland development. J Mammary Gland Biol Neoplasia. 2000;5(2):227–41.
7. Sternlicht M. Key stages in mammary gland development: the cues that regulate ductal branching morphogenesis. Breast Cancer Res. 2006;8(1):201.
8. Tharmapalan P, Mahendralingam M, Berman HK, Khokha R. Mammary stem cells and progenitors: targeting the roots of breast cancer for prevention. EMBO J. 2019;38(14):e100852.
9. Lim E, Vaillant F, Wu D, Forrest NC, Pal B, Hart AH, Asselin-Labat ML, Gyorki DE, Ward T, Partanen A, et al. Aberrant luminal progenitors as the candidate target population for basal tumor development in BRCA1 mutation carriers. Nat Med. 2009;15(8):907–13.
10. Celia-Terrassa T. Mammary stem cells and breast Cancer stem cells: molecular connections and clinical implications. Biomedicines 2018, 6(2).
11. Cicalese A, Bonizzi G, Pasi CE, Faretta M, Ronzoni S, Giulini B, Brisken C, Minucci S, Di Fiore PP, Pelicci PG. The tumor suppressor p53 regulates polarity of self-renewing divisions in mammary stem cells. Cell. 2009;138(6):1083–95.
12. Chiche A, Moumen M, Petit V, Jonkers J, Medina D, Deugnier MA, Faraldo MM, Glukhova MA. Somatic loss of p53 leads to stem/progenitor cell amplification in both mammary epithelial compartments, basal and luminal. Stem Cells. 2013;31(9):1857–67.
13. Santoro A, Vlachou T, Luzi L, Melloni G, Mazzarella L, D'Elia E, Aobuli X, Pasi CE, Reavie L, Bonetti P, et al. p53 loss in breast Cancer leads to myc activation, increased cell plasticity, and expression of a mitotic signature with Prognostic Value. Cell Rep. 2019;26(3):624–e638628.
14. Zhang M, Behbod F, Atkinson RL, Landis MD, Kittrell F, Edwards D, Medina D, Tsimelzon A, Hilsenbeck S, Green JE, et al. Identification of tumor-initiating cells in a p53-null mouse model of breast cancer. Cancer Res. 2008;68(12):4674–82.
15. Golipour A, Myers D, Seagroves T, Murphy D, Evan GI, Donoghue DJ, Moorehead RA, Porter LA. The Spy1/RINGO family represents a novel mechanism regulating mammary growth and tumorigenesis. Cancer Res. 2008;68(10):3591–600.
16. Porter LA, Dellinger RW, Tynan JA, Barnes EA, Kong M, Lenormand JL, Donoghue DJ. Human speedy: a novel cell cycle regulator that enhances proliferation through activation of Cdk2. J Cell Biol. 2002;157(3):357–66.
17. Karaiskou A, Perez LH, Ferby I, Ozon R, Jessus C, Nebreda AR. Differential regulation of Cdc2 and Cdk2 by RINGO and cyclins. J Biol Chem. 2001;276(38):36028–34.
18. Lenormand JL, Dellinger RW, Knudsen KE, Subramani S, Donoghue DJ. Speedy: a novel cell cycle regulator of the G2/M transition. Embo J. 1999;18(7):1869–77.
19. McGrath DA, Fifield BA, Marceau AH, Tripathi S, Porter LA, Rubin SM. Structural basis of divergent cyclin-dependent kinase activation by Spy1/RINGO proteins. EMBO J 2017.
20. Fifield BA, Qemo I, Kirou E, Cardiff RD, Porter LA. The atypical cyclin-like protein Spy1 overrides p53-mediated tumour suppression and promotes susceptibility to breast tumourigenesis. Breast Cancer Res. 2019;21(1):140.
21. Al Sorkhy M, Ferraiuolo RM, Jalili E, Malysa A, Fratiloiu AR, Sloane BF, Porter LA. The cyclin-like protein Spy1/RINGO promotes mammary transformation and is elevated in human breast cancer. BMC Cancer. 2012;12:45.
22. Barnes EA, Porter LA, Lenormand JL, Dellinger RW, Donoghue DJ. Human Spy1 promotes survival of mammalian cells following DNA damage. Cancer Res. 2003;63(13):3701–7.
23. Cheng A, Gerry S, Kaldis P, Solomon MJ. Biochemical characterization of Cdk2-Speedy/Ringo A2. BMC Biochem. 2005;6:19.

24. Gastwirt RF, Slavin DA, McAndrew CW, Donoghue DJ. Spy1 expression prevents normal cellular responses to DNA damage: inhibition of apoptosis and checkpoint activation. J Biol Chem. 2006;281(46):35425–35.

25. McAndrew CW, Gastwirt RF, Donoghue DJ. The atypical CDK activator Spy1 regulates the intrinsic DNA damage response and is dependent upon p53 to inhibit apoptosis. Cell Cycle. 2009;8(1):66–75.

26. Ferraiuolo RM, Fifield BA, Hamm C, Porter LA. Stabilization of c-Myc by the atypical cell cycle regulator, Spy1, decreases efficacy of breast cancer treatments. Breast Cancer Res Treat. 2022;196(1):17–30.

27. Ke Q, Ji J, Cheng C, Zhang Y, Lu M, Wang Y, Zhang L, Li P, Cui X, Chen L, et al. Expression and prognostic role of Spy1 as a novel cell cycle protein in hepatocellular carcinoma. Exp Mol Pathol. 2009;87(3):167–72.

28. Lubanska D, Market-Velker BA, deCarvalho AC, Mikkelsen T, Fidalgo da Silva E, Porter LA. The cyclin-like protein Spy1 regulates growth and division characteristics of the CD133 + population in human glioma. Cancer Cell. 2014;25(1):64–76.

29. Zucchi I, Mento E, Kuznetsov VA, Scotti M, Valsecchi V, Simionati B, Vicinanza E, Valle G, Pilotti S, Reinbold R, et al. Gene expression profiles of epithelial cells microscopically isolated from a breast-invasive ductal carcinoma and a nodal metastasis. Proc Natl Acad Sci U S A. 2004;101(52):18147–52.

30. Fifield BA, Talia J, Stoyanovich C, Elliott MJ, Bakht MK, Basilious A, Samsoondar JP, Curtis M, Stringer KF, Porter LA. Cyclin-Like Proteins Tip Regenerative Balance in the Liver to Favour Cancer Formation. *Carcinogenesis* 2019.

31. Ferraiuolo RM, Tubman J, Sinha I, Hamm C, Porter LA. The cyclin-like protein, SPY1, regulates the ERalpha and ERK1/2 pathways promoting tamoxifen resistance. Oncotarget. 2017;8(14):23337–52.

32. Gonzalez L, Domingo-Muelas A, Duart-Abadia P, Nunez M, Mikolcevic P, Llonch E, Cubillos-Rojas M, Canovas B, Forrow SMA, Morante-Redolat JM, et al. The atypical CDK activator RingoA/Spy1 regulates exit from quiescence in neural stem cells. iScience. 2023;26(3):106202.

33. Lubanska D, Porter LA. The atypical cell cycle regulator Spy1 suppresses differentiation of the neuroblastoma stem cell population. Oncoscience 2014, epub www.impactjournals.com/oncoscience

34. Lubanska D, Qemo I, Byrne M, Matthews KN, Fifield BA, Brown J, da Silva EF, Porter LA. The cyclin-like protein SPY1 overrides reprogramming induced senescence through EZH2 mediated H3K27me3. Stem Cells. 2021;39(12):1688–700.

35. Jacks T, Remington L, Williams BO, Schmitt EM, Halachmi S, Bronson RT, Weinberg RA. Tumor spectrum analysis in p53-mutant mice. Curr Biol. 1994;4(1):1–7.

36. McLean AC, Valenzuela N, Fai S, Bennett SA. Performing vaginal lavage, crystal violet staining, and vaginal cytological evaluation for mouse estrous cycle staging identification. J Vis Exp 2012(67):e4389.

37. Prater M, Shehata M, Watson CJ, Stingl J. Enzymatic dissociation, flow cytometric analysis, and culture of normal mouse mammary tissue. Methods Mol Biol. 2013;946:395–409.

38. Hu Y, Smyth GK. ELDA: extreme limiting dilution analysis for comparing depleted and enriched populations in stem cell and other assays. J Immunol Methods. 2009;347(1–2):70–8.

39. Vargo-Gogola T, Heckman BM, Gunther EJ, Chodosh LA, Rosen JM. P190-B rho GTPase-activating protein overexpression disrupts ductal morphogenesis and induces hyperplastic lesions in the developing mammary gland. Mol Endocrinol. 2006;20(6):1391–405.

40. Di Tommaso P, Chatzou M, Floden EW, Barja PP, Palumbo E, Notredame C. Nextflow enables reproducible computational workflows. Nat Biotechnol. 2017;35(4):316–9.

41. Ewels PA, Peltzer A, Fillinger S, Patel H, Alneberg J, Wilm A, Garcia MU, Di Tommaso P, Nahnsen S. The nf-core framework for community-curated bioinformatics pipelines. Nat Biotechnol. 2020;38(3):276–8.

42. Krueger FJF, Ewels P, Afyounian E, Weinstein M, Schuster-Boeckler B, Hulselmans G. and sclamons: Felixkrueger/trimgalore: V0.6.10 - Add Default Decompression Path. In.

43. Dobin A, Davis CA, Schlesinger F, Drenkow J, Zaleski C, Jha S, Batut P, Chaisson M, Gingeras TR. STAR: ultrafast universal RNA-seq aligner. Bioinformatics. 2013;29(1):15–21.

44. Patro R, Duggal G, Love MI, Irizarry RA, Kingsford C. Salmon provides fast and bias-aware quantification of transcript expression. Nat Methods. 2017;14(4):417–9.

45. Subramanian A, Tamayo P, Mootha VK, Mukherjee S, Ebert BL, Gillette MA, Paulovich A, Pomeroy SL, Golub TR, Lander ES, et al. Gene set enrichment analysis: a knowledge-based approach for interpreting genome-wide expression profiles. Proc Natl Acad Sci U S A. 2005;102(43):15545–50.

46. Wickham H. ggplot2: Elegant Graphics for Data Analysis. In: *Use R!* 2nd edn. Cham: Springer International Publishing: Imprint: Springer,; 2016: 1 online resource (XVI, 260 pages 232 illustrations, 140 illustrations in color.

47. Godar S, Ince TA, Bell GW, Feldser D, Donaher JL, Bergh J, Liu A, Miu K, Watnick RS, Reinhardt F, et al. Growth-inhibitory and tumor- suppressive functions of p53 depend on its repression of CD44 expression. Cell. 2008;134(1):62–73.

48. Love MI, Huber W, Anders S. Moderated estimation of Fold change and dispersion for RNA-seq data with DESeq2. Genome Biol. 2014;15(12):550.

49. Ponnaiya B, Cornforth MN, Ullrich RL. Radiation-induced chromosomal instability in BALB/c and C57BL/6 mice: the difference is as clear as black and white. Radiat Res. 1997;147(2):121–5.

50. Ullrich RL, Bowles ND, Satterfield LC, Davis CM. Strain-dependent susceptibility to radiation-induced mammary cancer is a result of differences in epithelial cell sensitivity to transformation. Radiat Res. 1996;146(3):353–5.

51. Asselin-Labat ML, Vaillant F, Sheridan JM, Pal B, Wu D, Simpson ER, Yasuda H, Smyth GK, Martin TJ, Lindeman GJ, et al. Control of mammary stem cell function by steroid hormone signalling. Nature. 2010;465(7299):798–802.

52. Fu NY, Nolan E, Lindeman GJ, Visvader JE. Stem cells and the differentiation Hierarchy in Mammary Gland Development. Physiol Rev. 2020;100(2):489–523.

53. Pece S, Tosoni D, Confalonieri S, Mazzarol G, Vecchi M, Ronzoni S, Bernard L, Viale G, Pelicci PG, Di Fiore PP. Biological and molecular heterogeneity of breast cancers correlates with their cancer stem cell content. Cell. 2010;140(1):62–73.

54. Vassilev LT, Vu BT, Graves B, Carvajal D, Podlaski F, Filipovic Z, Kong N, Kammlott U, Lukacs C, Klein C, et al. In vivo activation of the p53 pathway by small-molecule antagonists of MDM2. Science. 2004;303(5659):844–8.

55. Berger C, Qian Y, Chen X. The p53-estrogen receptor loop in cancer. Curr Mol Med. 2013;13(8):1229–40.

56. Berger CE, Qian Y, Liu G, Chen H, Chen X. p53, a target of estrogen receptor (ER) alpha, modulates DNA damage-induced growth suppression in ER-positive breast cancer cells. J Biol Chem. 2012;287(36):30117–27.

57. Jensen BV, Johansen JS, Price PA. High levels of serum HER-2/neu and YKL-40 independently reflect aggressiveness of metastatic breast cancer. Clin Cancer Res. 2003;9(12):4423–34.

58. Bernardo GM, Lozada KL, Miedler JD, Harburg G, Hewitt SC, Mosley JD, Godwin AK, Korach KS, Visvader JE, Kaestner KH, et al. FOXA1 is an essential determinant of ERalpha expression and mammary ductal morphogenesis. Development. 2010;137(12):2045–54.

59. Anderson LH, Boulanger CA, Smith GH, Carmeliet P, Watson CJ. Stem cell marker prominin-1 regulates branching morphogenesis, but not regenerative capacity, in the mammary gland. Dev Dyn. 2011;240(3):674–81.

60. Taifour T, Attalla SS, Zuo D, Gu Y, Sanguin-Gendreau V, Proud H, Solymoss E, Bui T, Kuasne H, Papavasiliou V, et al. The tumor-derived cytokine Chi3l1 induces neutrophil extracellular traps that promote T cell exclusion in triple-negative breast cancer. Immunity. 2023;56(12):2755–e27722758.

61. Tachi K, Shiraishi A, Bando H, Yamashita T, Tsuboi I, Kato T, Hara H, Ohneda O. FOXA1 expression affects the proliferation activity of luminal breast cancer stem cell populations. Cancer Sci. 2016;107(3):281–9.

62. Wright MH, Calcagno AM, Salcido CD, Carlson MD, Ambudkar SV, Varticovski L. Brca1 breast tumors contain distinct CD44+/CD24- and CD133 + cells with cancer stem cell characteristics. Breast Cancer Res. 2008;10(1):R10.

Publisher's Note